brief communication

Stroboscopic nuclear magnetic resonance microscopy of arterial blood flow

Ronald W. Behling, Helen K. Tubbs, Michael D. Cockman, and Lynn W. Jelinski
AT&T Bell Laboratories, Murray Hill, New Jersey 07974 USA

ABSTRACT NMR microscopy was used to obtain transverse flow profiles of arterial blood flow in the rat carotid artery at 33 μm resolution. The images were gated to the EKG and correspond to identified regions of diastole. The profiles show that flow is laminar during this part of the heart cycle. These results provide the first direct view of blood flow profiles in arteries of submillimeter diameter and suggest that animals as small as juvenile rodents will serve as valuable models for hemodynamic studies. Extensions to flow during systole, stenoses, and flow in the vicinity of the carotid bifurcation are discussed.

INTRODUCTION

Characterization of fluid flow is important in a wide variety of sciences, including analytical chromatography, reaction injection molding, botanical water transport, and medicine. Particularly in medicine, the visualization of blood flow is essential for characterizing normal and pathological states. In this report we show that stroboscopically sampled micromagnetic resonance imaging (micro-MRI) can be extended (Behling et al., 1989) to measure rapid arterial blood flow profiles in very small diameter 600–800 μm) arterial blood vessels in biologically accessible times. We furthermore show that flow is laminar at identified parts of the heart cycle. Considerations for obtaining optimum signal-to-noise under flow conditions are discussed and comparisons are made to gradient echo images.

Shortly after its discovery (Lauterbur, 1973), it was recognized that MRI could provide noninvasive information about fluid flow and about liquid diffusion. In the past decade a variety of schemes have been devised to measure flow. These include injecting a bolus of D_2O and performing deuterium NMR measurements (Ackerman et al., 1987; Kim and Ackerman, 1988), subtraction techniques that provide angiogram-like images of the cardiovascular system (Wedeen et al., 1985), phase images of slow venous blood flow (Pettigrew et al., 1987), influx of water into polymers and ceramics (Rothwell et al., 1984), and water diffusion and transport in plants (Jenner et al., 1988; Bottomley et al., 1986).

Spin-echo MRI can be used to measure flow in two different ways. The first involves time-of-flight considerations (Rittgers et al., 1988). Here, the flowing fluid, originally excited by the slice-selection pulse, either partially or completely flows out of the slice during the spin-echo time, leading to an intensity loss. This intensity loss is related to the flow rate, the echo time, T_E, and the slice thickness. The second basic method is based on the fact that the excited spins of a flowing fluid accumulate phase as they flow along a magnetic field gradient (Walker et al., 1988). The velocity is thus directly related to the phase angle. One can produce a phase-angle image where each pixel corresponds to the phase angle of the Fourier transform, given by the inverse tangent of the ratio of the imaginary and real data ($\tan^{-1}[I(f)/R(f)]$) (Brigham, 1974).

Although the phase angle image method is advantageous because only one image need be acquired, it suffers from signal-to-noise limitations when the flow is rapid. Rapid flow provides excellent contrast between flowing blood and the surrounding tissue because there is an *absence* of signal in the vessel, since the excited spins have flowed out of the slice before echo acquisition. However, the results presented here require the *presence* of a signal inside the artery. The experimental conditions used in this work (T_E = 20 ms, slice thickness = 800 μm), correspond to a flow rate cut-off of ~8 cm/s, above which flow cannot be observed. The flow during systole (approximately the first third of the heart cycle) in rats is too fast to be captured under these conditions; however, the flow at various points during diastole (the remaining two-

Dr. Behling's present address is Squibb Institute for Medical Research, Princeton, NJ 08543.

Dr. Tubbs's present address is Cornell Medical School, New York, NY 10021. Address correspondence to Dr. Jelinski, AT&T Bell Laboratories, 600 Mountain Ave., Murray Hill, NJ 07974.

thirds of the heart cycle) is well within the window of observation.

MATERIALS AND METHODS

Approximately 80-g female Sprague-Dawley rats were anesthetized with ethyl carbamate (urethane, Sigma Chemical Co., St. Louis, MO) in 0.85% wt/vol saline using 850 mg/kg injected intraperitoneally, followed by 850 mg/kg injected subcutaneously behind the neck. The rats were intubated and a water-filled 10 mm × 1.35 mm (OD) capillary was inserted near the carotid artery as a marker for vertical positioning. Although after practice one can reliably position the rat in the probe and locate the carotid artery, the surgically implanted capillary is useful for obtaining unambiguous identification of the carotid artery when the field of view (FOV) is reduced. It is also useful as a control for the phase images *vide infra*. The incision was sutured and EKG leads were placed on the upper abdomen, well away from the surface coil, with the resultant electrocardiogram producing a V_3-like trace. The rat was placed head-down in a specially designed plastic rodent holder that was affixed to the probe. The temperature of the rats dropped to 31°C and stabilized there. They breathed an atmosphere of 60% oxygen and 40% nitrogen.

Either the *R* or the *S* wave of the EKG was used for gating. The output from the EKG was fed simultaneously to a frequency counter and to a model 485 oscilloscpe (Tektronix, Inc., Beaverton, OR). The "A gate" output from the oscilloscope was inverted and used to trigger the spectrometer. Because of the gating characteristics of the spectrometer and the oscilloscope, it was essential to use a short (microsecond) timebase on the oscilloscope. The spin-echo pulse sequence incoporated a time delay between the triggering and excitation. This delay was adjusted so that slice excitation corresponded to a known fraction of the heart cycle. The heart cycle was recorded periodically during each 13 min experiment and remained stable to within 3% during the 13-min experiment and ~10% during the typically 5 h required to acquire a series of data.

The NMR images were obtained using a spin-echo imaging sequence on a model AM 360 (Bruker Instruments, Inc., Billerica, MA) equipped with an NMR microscope accessory. The probe circuit was modified to accommodate a 1.4-cm-diameter, single-turn surface coil. A 2-ms lobeless sinc pulse was used for the slice-selective 90 and 180 $\check{C}$ pulses. The water linewidth was shimmed on the desired slice to ~100 hertz. The gradient strengths for the 33.9 × 33.9 × 0.8 mm FOV were 0.69, 0.74,

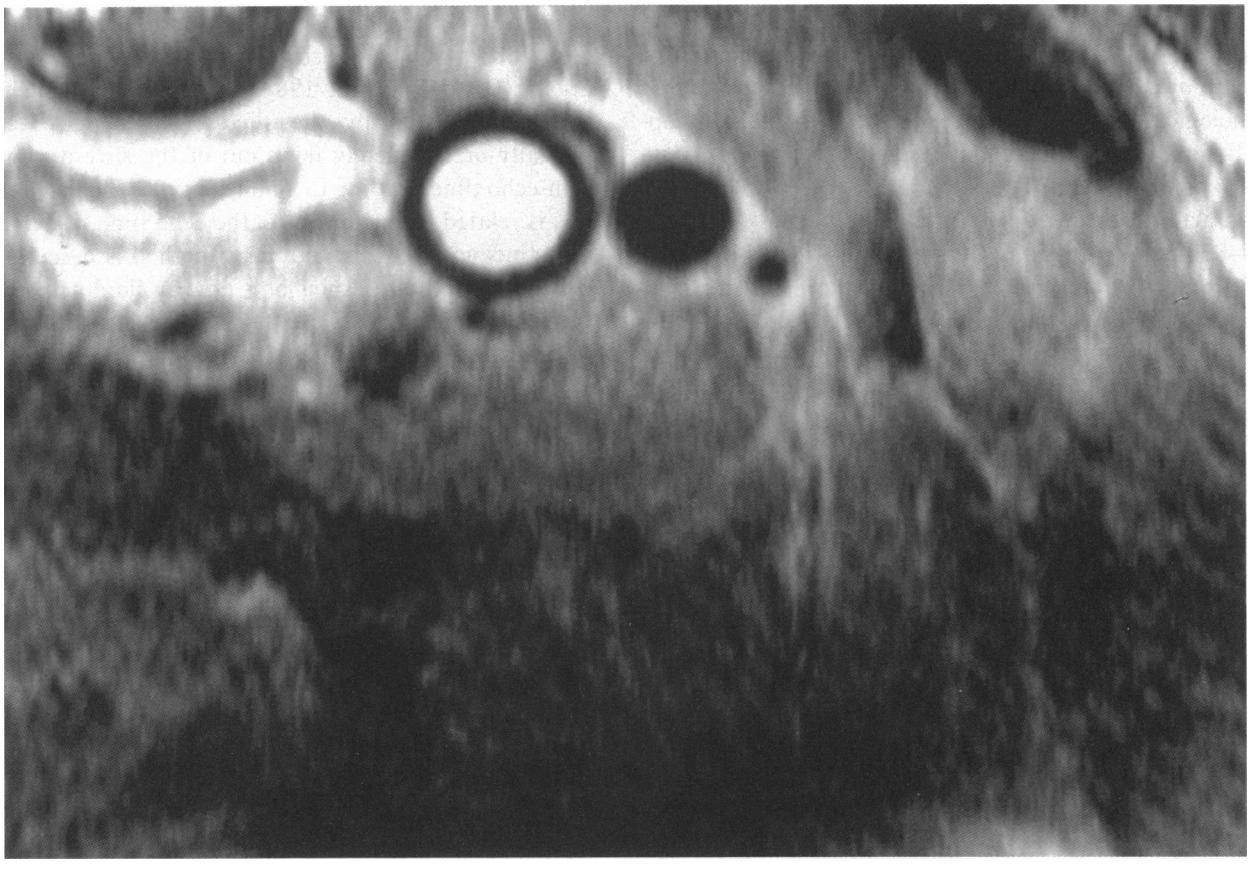

FIGURE 1 Gated transverse NMR image of the carotid artery of an 82-g rat. The field of view was 8.5 × 8.5 mm and the image corresponds to systole. The bright object is a saline-filled 10 × 1.35 mm (OD) glass capillary that was inserted near the carotid artery as a marker. The carotid artery is the ~800-μm dark object directly to the right of the marker. A smaller collateral artery (~50 μm) is also visible in this image. Parts of the trachea (*upper left*) and jugular vein (*upper right*) are also visible in this image.

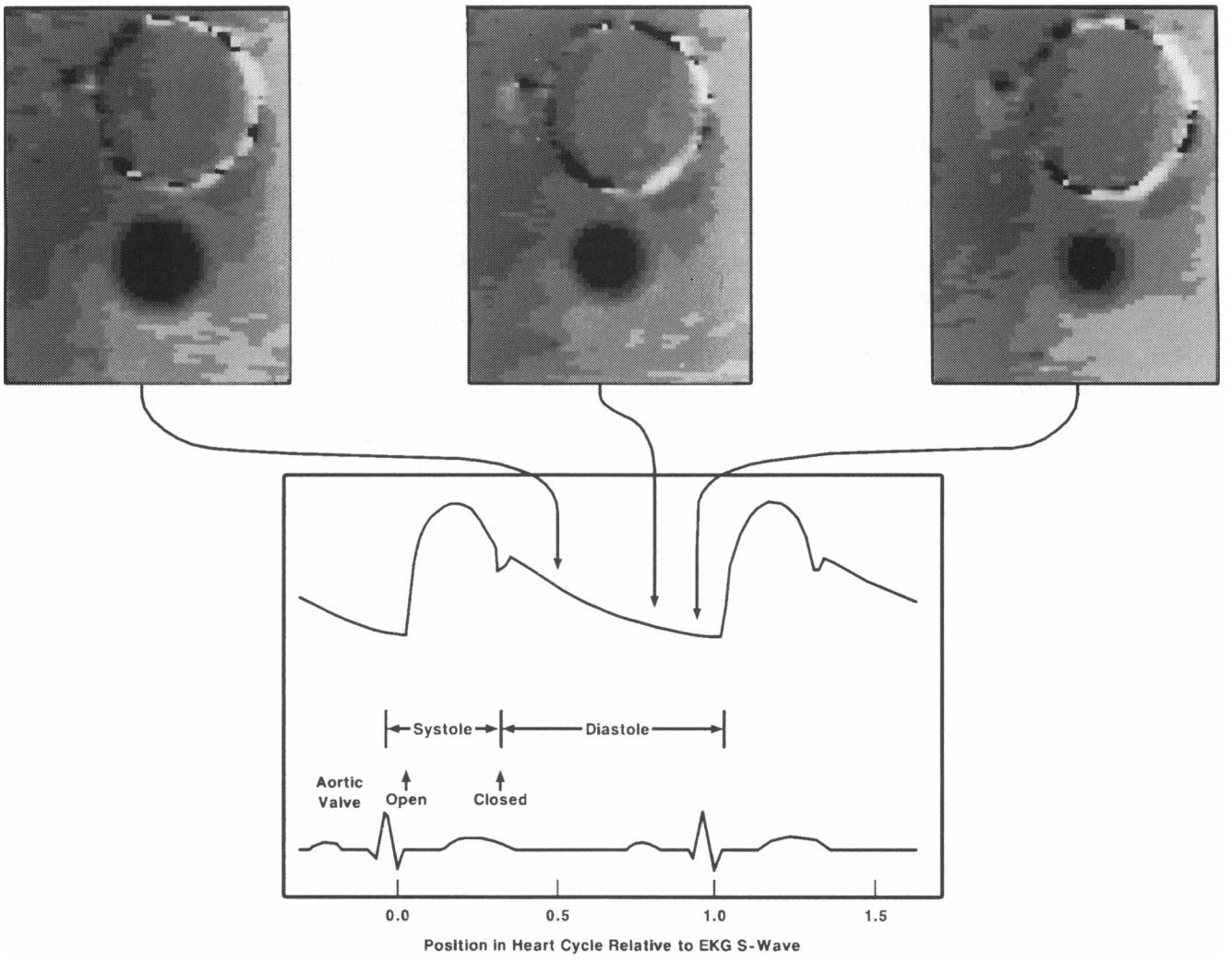

FIGURE 2 Phase images corresponding to various fractions (0.49, 0.77, and 0.91) of the heart cycle. The heart period was monitored three times during each image acquisition and was 158 ± 3 ms. The object at the top of the images is the water-filled marker. The liquid in the marker is not flowing and the liquid in the marker therefore reflects the level of noise and uncertainty of phasing in these images. The carotid, with its phase flow information, is the object directly below the marker. The gray scale corresponds to flow velocity.

and 1.8 Gauss/cm for the read-out (x), phase-encode (y), and slice-select (z) directions, respectively. For the 8.5 × 8.5 × 0.8 mm field of view the gradient strengths were 2.77, 1.48, and 1.8 Gauss/cm, respectively. The images consist of two scans of 256 points at each of 64 phase-encode increments surrounding the echo maximum. The repetition time (T_R) was 6 s. Although only 64 phase-encode increments were used, the size of the increment corresponded to the reduced FOV (i.e., whether using 256 or 64 phase encode gradients, the phase encode *increment* remained unchanged). 90° tip angles were used. The echo time (T_E) was set at 20 ms. The pixel size in the phase-encode direction was 132 and 33 μm in the read direction before zero filling. Slice thickness was ~800 μm.

Signal aliasing ("folding") in both dimensions must be tolerated to obtain images at the smaller field of view. Folding is less of a problem with a surface coil than with a volume coil because the signal from the surface coil drops off rapidly more than a radius distant from the coil. All images were carefully checked to ensure that folded-in signals did not affect the signals from the carotid artery or the marker.

The data were processed on a VAXStation II using version 4.9 of FTNMR from Dennis Hare. The data matrix was zero filled to 512 × 512 before Fourier transformation; no signal enhancement or digital filtering was applied to the data. Because we collected echoes that were not centered within the acquisition window, large first-order phase corrections were required. The phase image was constructed by taking the inverse tangent of the angle between the imaginary and real data for each voxel. Velocities were determined using the equation:

$$v_z = 0.048\phi_z,$$

where v_z is the velocity along the z-direction in cm/s and ϕ_z is the phase

angle in degrees. This method of determining flow velocities was verified using a calibrated flow phantom.

RESULTS AND DISCUSSION

Fig. 1 shows a typical micro-MRI image of the carotid artery, gated so the image corresponds to the peak of systole. The bright object surrounded by the dark rim is the 1.35-mm OD saline-filled glass marker. The fully-expanded carotid artery is immediately to the right of the marker, and a smaller collateral artery appears on the right side of the carotid. A portion of the trachea is also visible on the upper left of Fig. 1, and part of the jugular vein appears on the upper right. Data of the high resolution shown in Fig. 1 require that extreme attention be paid to all details of the imaging experiment. This includes signal-to-noise considerations and shimming on the slice that will be examined. The gating must be reliable and the echo time as short as possible. Breathing artifacts were not a problem because the rat was sufficiently immobilized. The artery appears dark in this image because it corresponds to the extreme peak of systole, where essentially all of the originally excited blood had flowed out of the artery before the echo was acquired.

We have previously shown that we can map the dimensional changes of the carotid artery over the entire heart cycle and have furthermore demonstrated a noninvasive method for measuring Young's modulus of the artery from the NMR data (Behling et al., 1989). Having demonstrated the ability to obtain images that correspond to clearly identified parts of the heart cycle, we now obtain and analyze images to obtain noninvasive profiles of blood flow. Examples of such images are shown in Fig. 2, where three phase-images are displayed above an idealized blood pressure waveform. The outline of the water-filled marker appears at the top of each of these images. Because there is no flow in the liquid in the marker, there should be no phase variation across the marker. The small amount of phase variation that is observed reflects sources of phase such as magnetic field and RF inhomogeneity. The carotid is the dark object directly below the marker, where the effects of flow are observed directly. Here the gray scale corresponds to flow velocity. (Explicit flow velocities are summarized below.)

The data of Fig. 2 can be plotted in perspective form rather than with gray scales; these are shown in Fig 3. The three perspectives correspond directly to the carotid artery region of the data shown in Fig. 2; the vertical axis corresponds to the flow velocity. These data appear to map out a parabolic flow profile. Investigation of slices taken from Fig. 3 show that the flow is fairly symmetrically disposed about the artery. Cross-sections at the position of maximum flow (approximately at the midpoint of the artery) are shown in Fig. 4 (*solid lines*). The sloping baseline, seen in Fig. 2, was assumed to arise from sources of phase other than flow and was subtracted for this figure. These data have been fit to a parabola (*dotted lines*) showing that the flow is indeed laminar. The maximum flow velocities at 0.49, 0.77, and 0.91 of the heart cycle are 7.5, 6.0, and 4.0 cm/s, respectively.

These experiments are not without difficulties and further technical advances must be attained for a more complete realization of the initial work presented here. For example, the T_E in the spin-echo sequence imposes a finite cut-off time, and the T_E of 20 ms used in these experiments is too long to capture the rapid blood flow during systole. Using a variety of techniques, including actively shielded gradients, one could perhaps reduce the

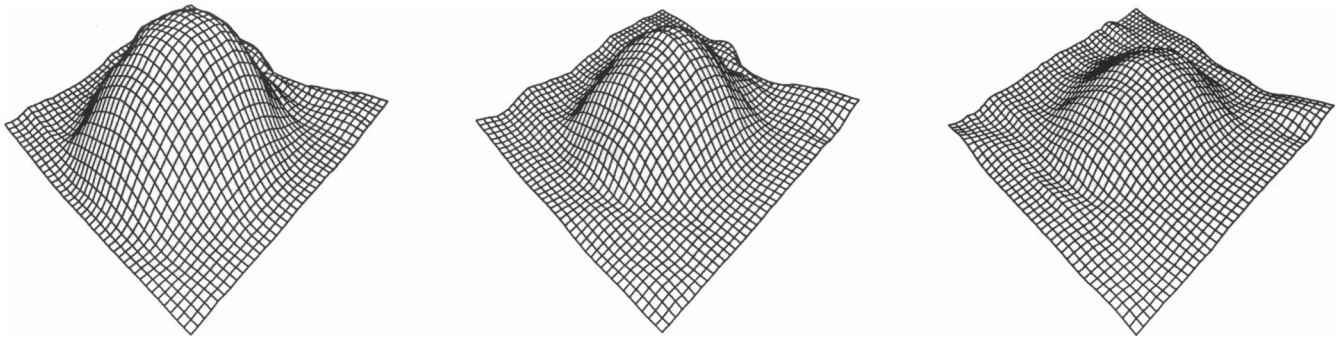

FIGURE 3 Perspective drawings of the blood flow data presented in Fig. 2. The vertical axis corresponds to velocity; the velocity scale is shown explicitly in Fig. 4.

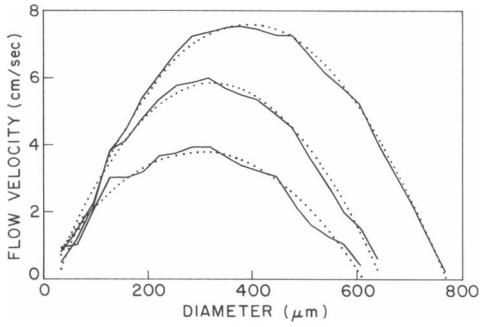

FIGURE 4 Blood flow velocity as a function of position across the carotid artery. The three solid lines correspond to the data of Fig. 3 after the sloping baseline was subtracted out. These represent data from fractional positions in the heart cycle of 0.49, 0.77, and 0.91. The dotted lines are a fit to a parabola ($y = ax^2 + b$).

T_E to at least half its present value. We have investigated the alternative approach of using a gradient echo instead of the spin-echo sequence used in this work. Although one can capture images throughout the entire heart cycle, we find that the gradient echo under flow conditions is especially sensitive to the effects of magnetic field inhomogeneities and that the images are difficult to phase.

These results provide the first direct view of blood flow profiles in arteries of submillimeter diameter. They demonstrate that stroboscopically sampled MRI can provide direct and detailed information about blood flow patterns. The blood flow pattern in the carotid artery was laminar throughout diastole. These results are significant for several reasons. First, they demonstrate that animals as small as juvenile rats are suitable as models for hemodynamic investigations. The ability to use rodents for such studies reduces the cost and complexity of performing experiments on blood flow. Furthermore, these experiments provide the groundwork for important extensions investigating blood flow in the presence of stenoses, near occlusions, and in the vicinity of the carotid bifurcation.

Received for publication 6 October 1989 and in final form 13 March 1990.

REFERENCES

Ackerman J. J. H., C. S. Ewy, N. N. Becker, and R. A. Shalwitz. 1987. Deuterium nuclear magnetic resonance measurements of blood flow and tissue perfusion employing ^2H_2O as a freely diffusible tracer. *Proc. Natl. Acad. Sci. USA.* 84:4099–4102.

Behling R. W., H. K. Tubbs, M. D. Cockman, and L. W. Jelinski. 1989. Stroboscopic NMR microscopy of the carotid artery. *Nature (Lond.).* 340:321–322.

Bottomley, P. A., H. H. Rogers, and T. H. Foster. 1986. NMR imaging shows water distribution and transport in plant root systems in situ. *Proc. Natl. Acad. Sci. USA* 83:87–89.

Brigham, E. O. 1974. The Fast Fourier Transform. Prentice-Hall, Inc., Englewood Cliffs, NJ. 12.

Jenner, C.F., Y. Xia, C. D. Eccles, and P. T. Callaghan. 1988. Circulation of water within wheat grain revealed by nuclear magnetic resonance micro-imaging. *Nature (Lond.).* 336:399–402.

Kim, S.-G., and J. J. H. Ackerman. 1988. Multicompartment analysis of blood flow and tissue perfusion employing D_2O as a freely diffusible tracer: a novel deuterium NMR technique demonstrated via application with murine RIF-1 tumors. *Magn. Res. Med.* 8:410–426.

Lauterbur, P. C. 1973. Image formation by induced local interactions: examples employing nuclear magnetic resonance. *Nature (Lond.).* 242:190–191.

Pettigrew, R. I., W. Dannels, J. R. Galloway, T. Pearson, W. Millikan, J. M. Henderson, J. Peterson, and M. E. Bernardino. 1987. Quantitative phase-flow MR imaging in dogs by using standard sequences. *Am. J. Roentgeneol.* 148:411–414.

Rittgers, S. E., D.-y. Fei, K. A. Kraft, P. P. Fatouros, and P. R. S. Kishore. 1988. Velocity profiles in stenosed tube models using magnetic resonance imaging. *Trans. ASME (Am. Soc. Mech. Eng.) J. Biomech. Eng.* 110:180–184.

Rothwell, W. P., D. R. Holecek, and J. A. Kershaw. 1984. NMR imaging. Study of fluid absorption by polymer composites. *J. Polym. Sci. Polym. Lett. Ed.* 22:241–247.

Walker, M. F., S. P. Souza, and C. L. Dumoulin. 1988. Quantitative flow measurement in phase contrast MR angiography. *J. Comp. Assisted Tomogr.* 12:304–313.

Wedeen, V. J., R. A. Meuli, R. R. Edelman, S. C. Geller, L. R. Frank, T. J. Brady, and B. R. Rosen. 1985. Projective imaging of pulsatile flow with magnetic resonance. *Science (Wash. DC).* 230:946–948.